PROCEEDINGS OF ASME TURBO EXPO 2015: TURBINE TECHNICAL CONFERENCE AND EXPOSITION
GT2015
JUNE 15 – 19, 2015, MONTRÉAL, CANADA

ASME GT2015-43389

EFFECTS OF UNSTEADY FLOW INTERACTIONS ON THE PERFORMANCE OF A HIGHLY-LOADED TRANSONIC COMPRESSOR STAGE

Chunill Hah
NASA Glenn Research Center,
MS 5-10, Cleveland, Ohio

ABSTRACT

The primary focus of this paper is to investigate the loss sources in an advanced GE transonic compressor design with high reaction and high stage loading. This advanced compressor has been investigated both experimentally and analytically in the past. The measured compressor efficiency is significantly lower than the efficiency calculated with various existing tools based on RANS and URANS. The general understanding is that some important flow physics in this modern compressor design are not represented in the current tools. To pinpoint the source of the efficiency miss, an advanced test with detailed flow traverse was performed for the front one and a half stage at the NASA Glenn Research Center. In the present paper, a Large Eddy Simulation (LES) is employed to determine whether a higher-fidelity simulation can pick up any additional flow physics that can explain past efficiency miss with RANS and URANS. The results from the Large Eddy Simulation were compared with the NASA test results and the GE interpretation of the test data. LES calculates lower total pressure and higher total temperature on the pressure side of the stator, resulting in large loss generation on the pressure side of the stator. On the other hand, existing tools based on the RANS and URANS do not calculate this high total temperature and low total pressure on the pressure side of the stator. The calculated loss through the stator from LES seems to match the measured data and the GE data interpretation. Detailed examination of the unsteady flow field from LES indicates that the accumulation of high loss near the pressure side of the stator is due to the interaction of the rotor wake with the stator blade. The strong rotor wake interacts quite differently with the pressure side of the stator than with the suction side of the stator blade. The concave curvature on the pressure side of the stator blade increases the mixing of the rotor wake with the pressure side boundary layer significantly. On the other hand, the convex curvature on the suction side of the stator blade decreases the mixing and the suction side blade boundary layer remains thin. The jet velocity in the rotor wake in the stator frame seems to magnify the curvature effect in addition to inviscid redistribution of wake fluid toward the pressure side of the blade.

INTRODUCTION

The recent drive to increase the efficiency of large gas turbine engines demands the development of advanced high pressure ratio core compressors. It is well known that the current generation of CFD tools based on RANS and URANS overpredicts the efficiency of such high pressure ratio transonic compressor stages. It is generally believed that some of the flow physics inside such a highly loaded compressor stage are not properly captured with these analytical tools. A test was performed at the NASA Glenn Research Center to pinpoint the source of loss with an advanced GE compressor design. The results, reported by Prahst et al. [2015], show that front stage efficiency is significantly lower than RANS and URANS calculations. Evaluation and detailed data match analysis of the measured data are reported by Lurie and Breeze-Stringfellow [2015]. The current paper reports a parallel investigation to examine the flow field with a higher fidelity analysis tool (LES) to capture any relevant flow physics.

Many significant research works have been reported on the loss generation inside multistage turbomachinery. Smith [1966] explained that rotor wake stretching in the stator can provide some total pressure recovery in his widely referred classical paper. Van Zante et al [2002] examined this wake recovery effect in a high speed axial compressor. Kerrebrock and Mikolajczk [1970] pointed out that the rotor wake has higher total pressure and higher total temperature in absolute

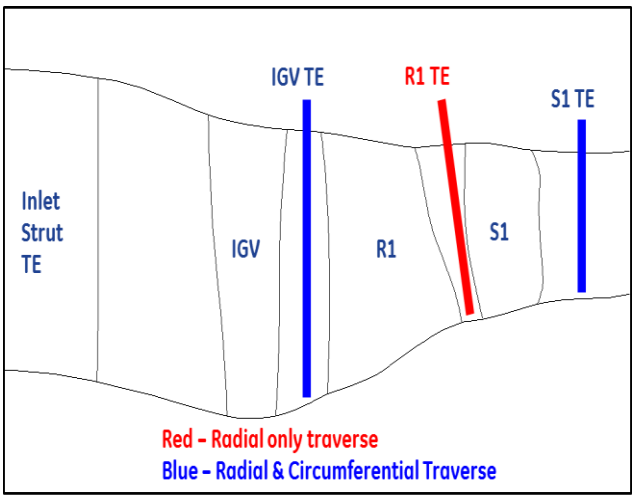

Figure 1: Cross section of test compressor and detailed traverse locations

frame than those in the free stream and the rotor wake is convected to the pressure side of the stator.

RANS and URANS have been widely used for the design and analysis of compressor/turbine stages. A 1-2% efficiency improvement is attributed to these analysis tools (Smith [2010]). However, recent studies (for example, Hah and Katz [2014]) found that generation, transport, and interactions of vortices in turbomachinery are not well calculated by RANS and URANS. Modeling of all the turbulence scales in the entire field with a single length scale might be one of reasons for this behavior. Recently, higher fidelity analysis tools based on Direct Numerical simulation (DNS) and LES are being introduced for turbomachinery flow analysis (Zaki et al. [2010], Hah et al. [2012], Gourdain [2013], Hah and Katz [2014], and Papadogiannis et al. [2014]). These high fidelity analysis tools require large scale computational resources and need further validation with suitable data sets.

TEST DATA AND LES SETUP

Figure 1 shows detailed traverse locations of the tested one and a half stage transonic axial compressor. The tested compressor stage is the front stage of a GE highly loaded and high reaction transonic core compressor. The traverses in Figure 1 consisteted of a 5–hole probe, stagnation Kulite probes, and hotwire probes to perform radial and circumferential traverses behind the IGV, Stator 1 (S1) and Rotor 1 (R1). Additionally, various fixed inter-stage instrumentations, including over-the-rotor Kulite and S1 leading edge total pressure and total temperature, were installed. Details of the test, data aquistion and data interpretation are given by Prahst et al. [2015] and Lurie and Breeze-Stringfellow [2015].

Figure 2 shows the computational domain and the grid topology for the LES analysis. As shown in Figure 2, the exit plane of the computational domain was placed about 10 S1 blade heights away to minimize pressure reflection from the exit plane. The inlet plane was located near the inlet strut trialing edge. Details of the LES process are given by Hah and Shin. [2012]. The subgrid stress tensor was modeled with the standard dynamic model by Germano et al. [1991]. A third-order accurate interpolation scheme is used for the convection term.

As is well known (for example, Padogiannis et al. [2014]), the LES solution depends on the grid size and requires long computation. To get converged unsteady flow field in a sigle stage compressor with URANS, the computation of 20 – 30 rotor revolutions might be required. On the other hand, LES might require as much as 100 - 200 rotor revolutions to obtain the periodic unsteady flow field. Influence of different models of the subgrid scale stress becomes less recognizable when the computational grid becomes finer. Susequently, the user's understanding and experience with any particular LES procedure are still very important factors in extracting useful physical insights from the LES simulation.

The actual number of blades in the current compressor is 42 IGV blades, 28 rotor blades, and 58 stator blades. To perform fine grid LES simulations of the stage with periodicity conditons in the tangential direction, the number

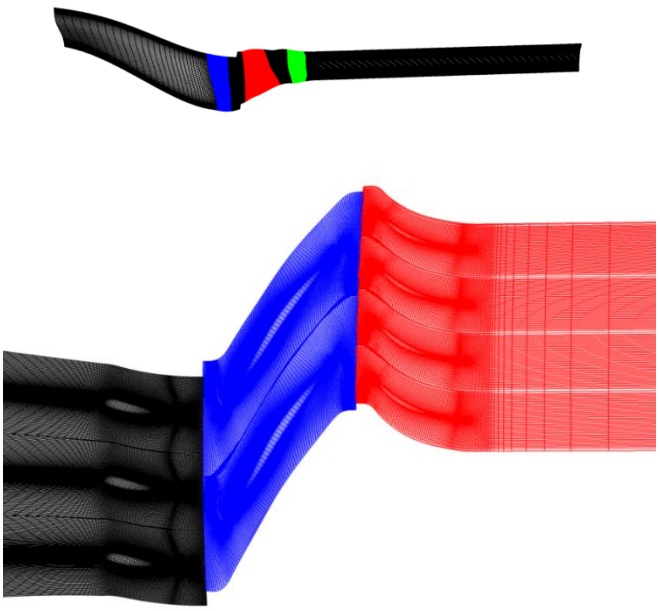

Figure 2: Computational domain and grid topology

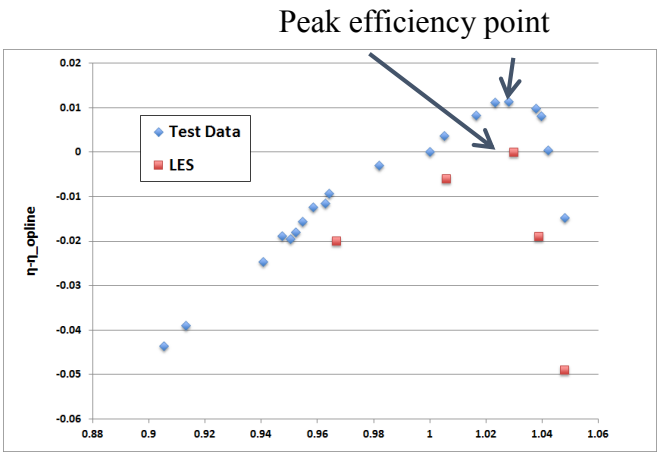

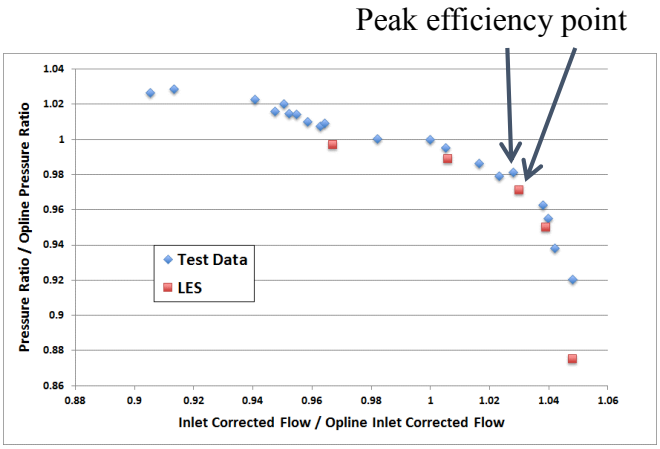

Figure 3: Comparison of corrected speedline relative to multi-stage compressor opline

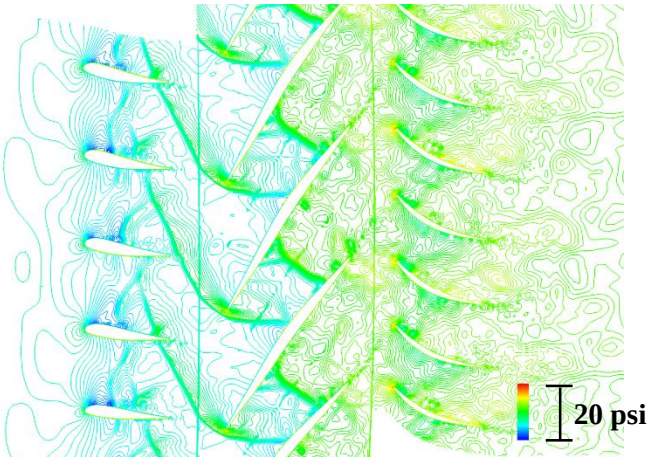

Figure 4: Instantaneous pressure distribution at mid-span

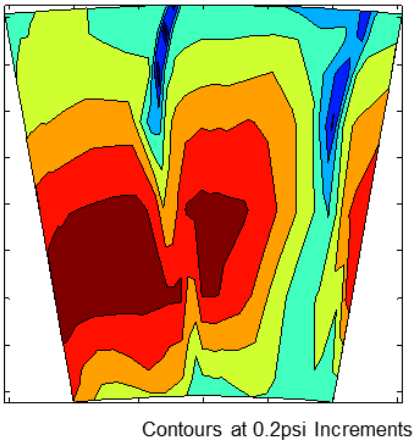

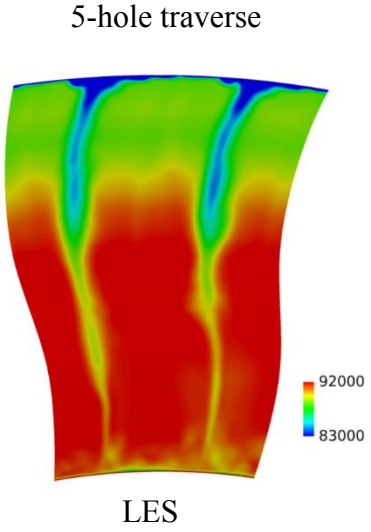

Figure 5: Comparison of total pressure distribution at the exit of IGV

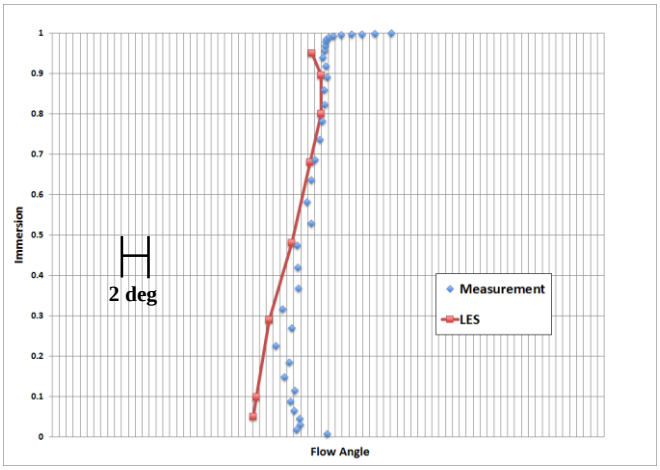

Figure 6: Comparison of IGV exit swirl angle

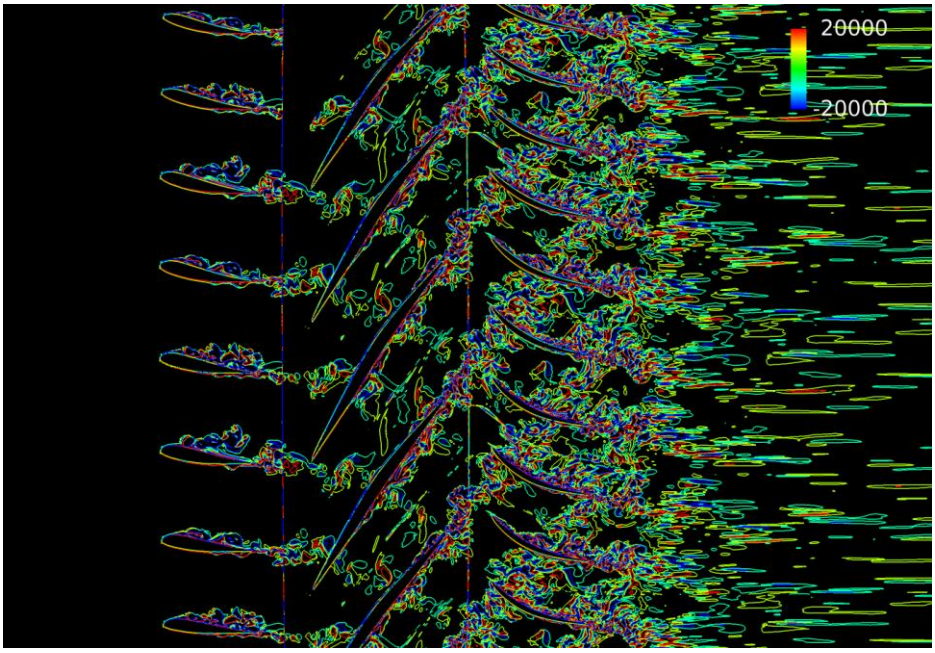

Figure 7: Instantaneous vorticity contours at mid-span

of stator blades was changed to 56 by scaling the stator blade. LES was performed with 3 IGV blades, 2 rotor blades and 4 stator blades which represents 1/14 of the machine passage. Various sizes of the computational grid were tested for the LES simulation. About 60 million grid nodes for the 7 blade passages (3 IGV + 2 R1+ 4 S1) gave incorrect flow field. The calculated unsteady flow with 60 million grid nodes showed a large flow separation on the suction side of the S1, which does not agree with the measured total pressure distribtuion at S1 exit. A total grid size of more than 300 million CFD nodes seems to give an acceptable unsteady flow field. The final computation was performed with 400 million grid nodes. The wall resolution is within the range of $Dx^+ < 20$, $Dy^+ < 1.0$, and $Dz^+ < 2.0$ in streamwise, pitchwise and the spanwise directions with the final computational grid. The current LES computation was used as an analysis tool to diagnose the flow field together with the state-of-the-art flow measurement. All the computations were performed with the NASA's Pleiades supercomputer system. With the 960 parallel processors, about 60 CPU hours are required for each compressor rotor revolution.

COMPRESSOR SPEEDLINE AND OVER ALL FLOW FIELD

Figure 3 shows measured and calculated corrected speedline of the compressor stage. LES calculates a slightly higher choke mass flow rate than the measurement. The mass flow rate in Figure 3 was corrected by the mass flow rate corresponding to the opline of the full machine. LES calculates lower pressure rise and lower compressor efficiency compared to the measurement. However, the overall trend of the compressor characteristics seems to be calculated properly. An instantaneous pressure field at the mid span is shown in Figure 4. As expected with the high rotor blade loading, strong flow interaction of the Rotor 1 shock with the IGV blade is shown in Figure 4. Calculated total pressure distribution at the exit of the IGV is compared with the measurement in Figure 5. Radial distribution of the IGV swirl angle is compared in Figure 6. The LES results in Figure 5 and 6 were obtained by time-averaging instantaneous flow fields over one rotor revolution. The flow behind the IGV is highly unsteady due to the IGV trailing edge vortex shedding, which is trigged by the shock wave from the Rotor 1. However, averaged total pressure and the swirl angle behind the IGV are calculated reasonably well. The clearance at the IGV hub was not modeled for the current simulation, which results in the discrepancy near the hub in Figure 6.

Instantaneous vorticity contours at the mid-span from LES are shown in Figure 7. Effects of shock induced vortices on performance in transonic compressors were investigated by Nolan et al. [2009] and Knobbe et al. [2013]. Both the current LES and the GE data match analysis by Lurie and Breeze-Stringfellow [2015] tell the loss through the IGV is small. The vorticity contours in Figure 7 do not indicate any strong IGV wake phasing on the rotor. LES simulations with wider spaces between the IGV and Rotor 1 did not show any appreciable change in the rotor performance. Radial distribution of the total pressure and the total temperature at the exit of Rotor 1 are compared in Figures 8 and 9. Calculated total pressure and total temperature match the

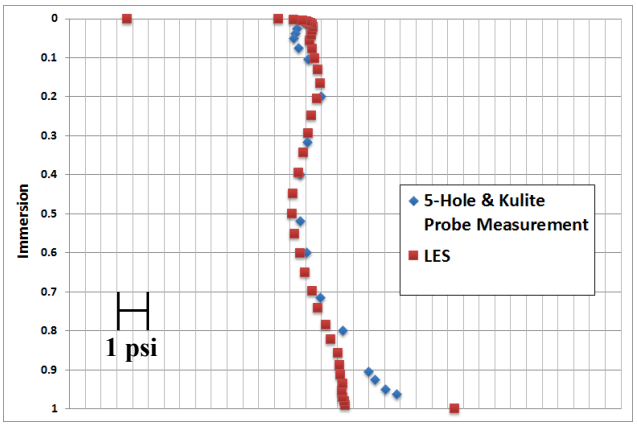

Figure 8: Comparison of radial distribution of total pressure at rotor exit

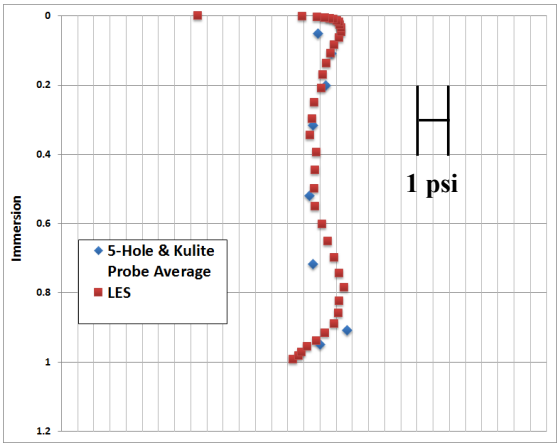

Figure 10: Comparison of radial distribution of total pressure at stator exit

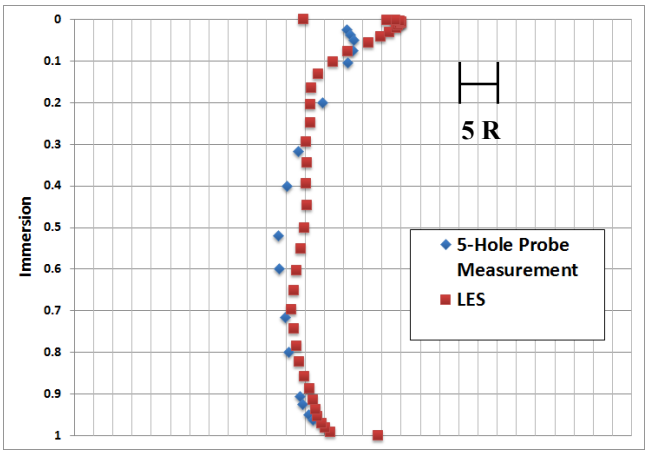

Figure 9: Comparison of total temperature distribution at rotor exit

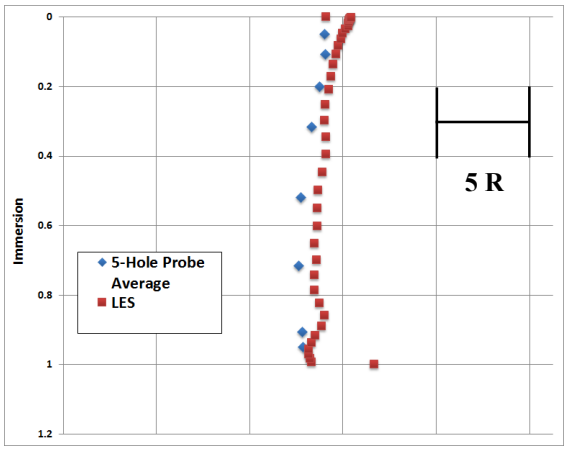

Figure 11: Comparison of radial distribution of total temperature at stator exit

measurements fairly well considering the possible uncertainty range in both the measurement and the simulation. The LES shows about two thirds of the overall loss occurs through the Rotor 1 exit plane in Figure 1. The flow field in this compressor has been investigated extensively with several different stage configurations and accompanying analysis tools. Based on the current detailed inter-stage measurements, detailed data analysis (Lurie and Breeze-String Fellow [2015]), and the present LES simulation, additional loss, which was not identified previously with RANS and URANS, was determined to occur through the Stator 1 passage.

ROTOR 1 WAKE INTERACTION WITH STATOR

The interaction of rotor wakes with stator blades in compressors has been studied extensively. Smith [1966] explained effects of wake stretching through the stator passage. Kerrbrock and Mikolajcak [1970] showed that rotor wake has higher total temperature in stator frame and accumulates on the pressure side of the stator.

The radial distribution of the total pressure and the total temperature at the S1 exit plane are compared in Figures 10 and 11. LES calculates the overall flow field reasonably well. Figure 12 compares total pressure contours at the S1 exit survey plane. The total pressure distribution from LES agrees fairly well with the measurement especially near the mid-span. Both the measurement and the LES show lower total pressure area in the pressure side of the stator, which was not identified previously. Calculated total temperature distribution at the Stator 1 exit plane is given in Figure 13. LES calculates higher total temperature and lower total pressure on the pressure side of the stator than those on the suction side, which indicates higher loss on the pressure side of the stator. Circumferential distribution of total pressure and the total temperature are compared in Figures 14 and 15. The

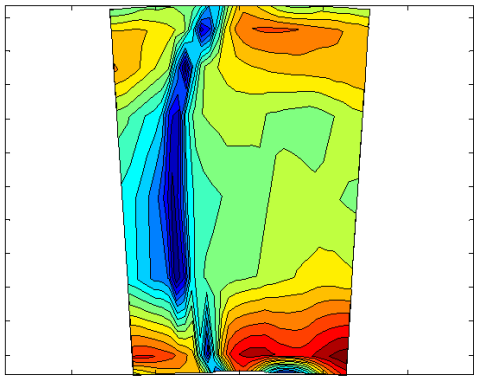

5-hole traverse

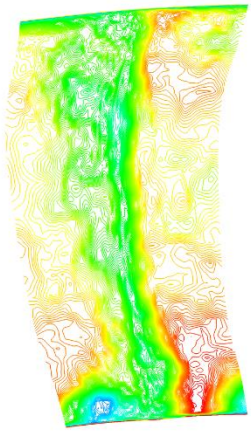

LES

Figure 12: Comparison of total pressure distribution at stator exit

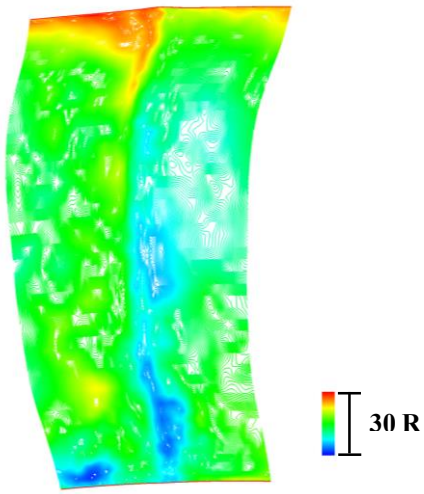

Figure 13: Total temperature distribution at stator exit from LES

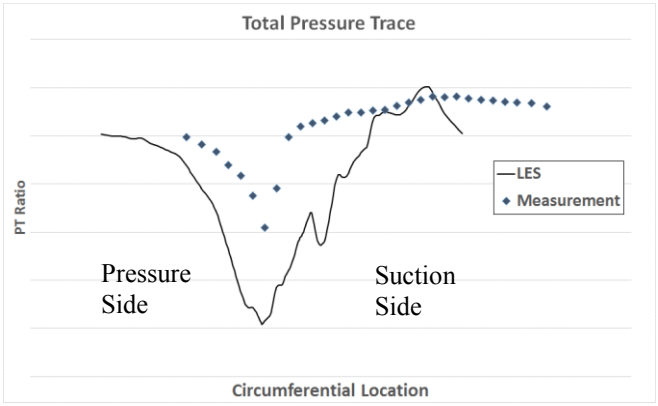

Figure 14: Comparison of total pressure circumferential distribution of total pressure at mid span

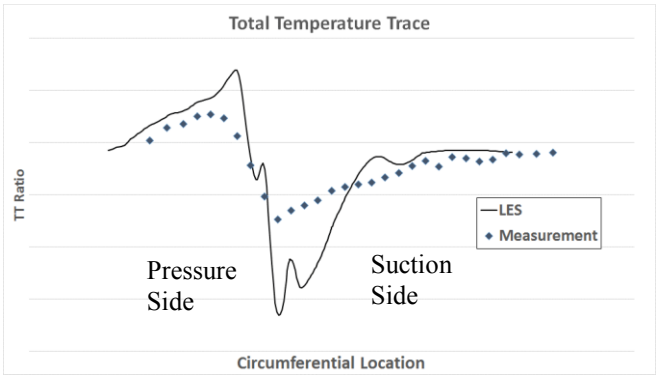

Figure 15: Comparison of circumferential distribution of total temperature at mid span

results shown in Figures 12 through 15 are due to unsteady flow in the stator. To identify the source of this high loss generation in the stator pressure side, the unsteady flow field from the LES was examined in detail.

Figure 16 shows instantaneous contours of tangential velocity through the stator. The vector diagram of the rotor wake flow relative to the free stream flow is also shown in Figure 16. As shown in the vector diagram in Figure 16, the rotor wake has an additional velocity component in the absolute stator frame. This additional velocity component in the wake (jet velocity) adds tangential velocity toward the pressure side of the blade. Kerrebrock and Mikolajczk [1970] explained that this additional velocity component (jet velocity) pushes the rotor wake with higher total temperature toward the pressure side. Instantaneous distribution of the tangential velocity component in Figure 16 shows a strong negative tangential velocity component in the rotor wake.

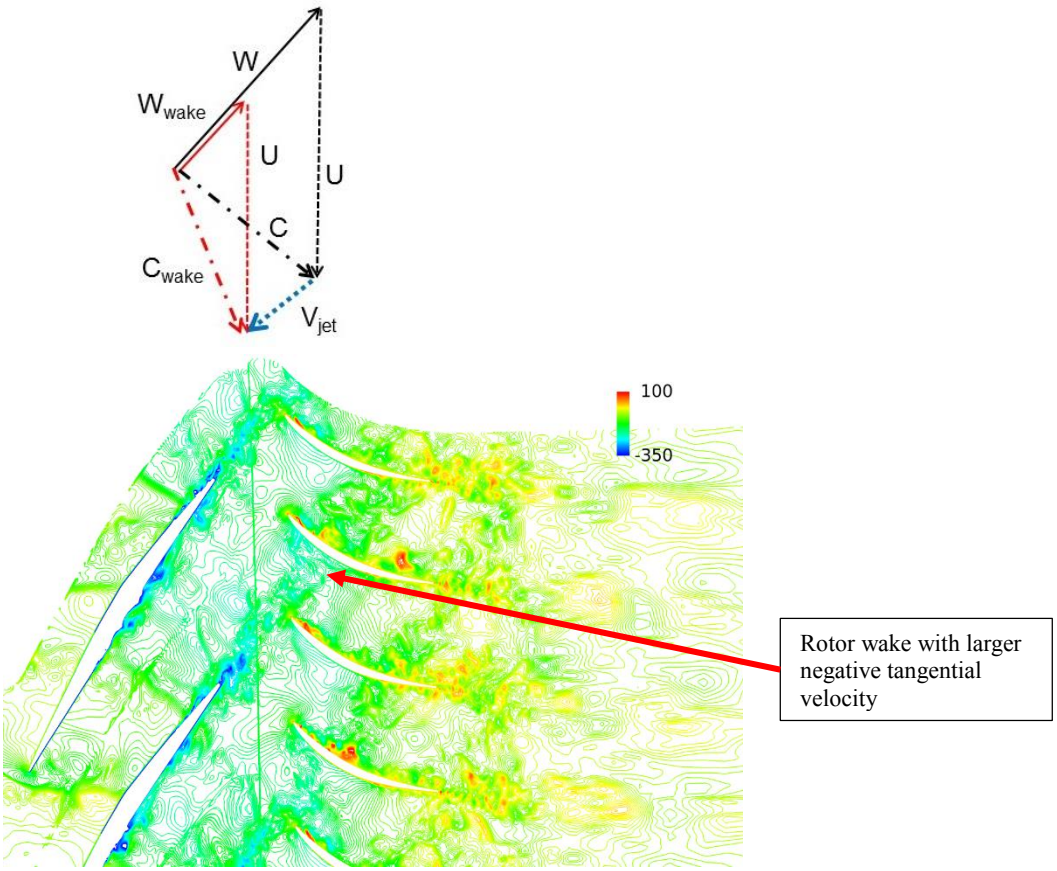

Figure 16: Instantaneous distribution of tangential velocity in stator passage

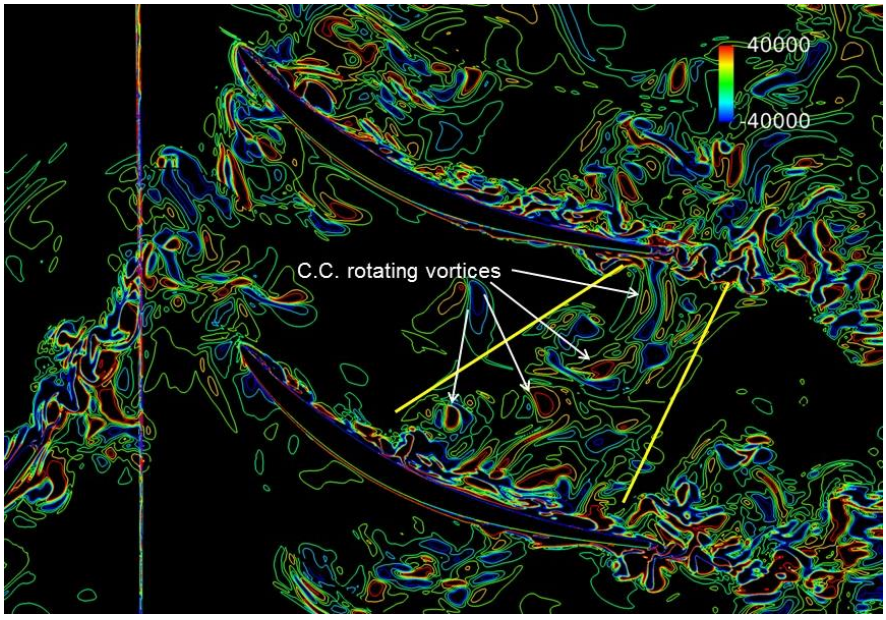

Figure 17: Instantaneous vorticity contours inside stator passage

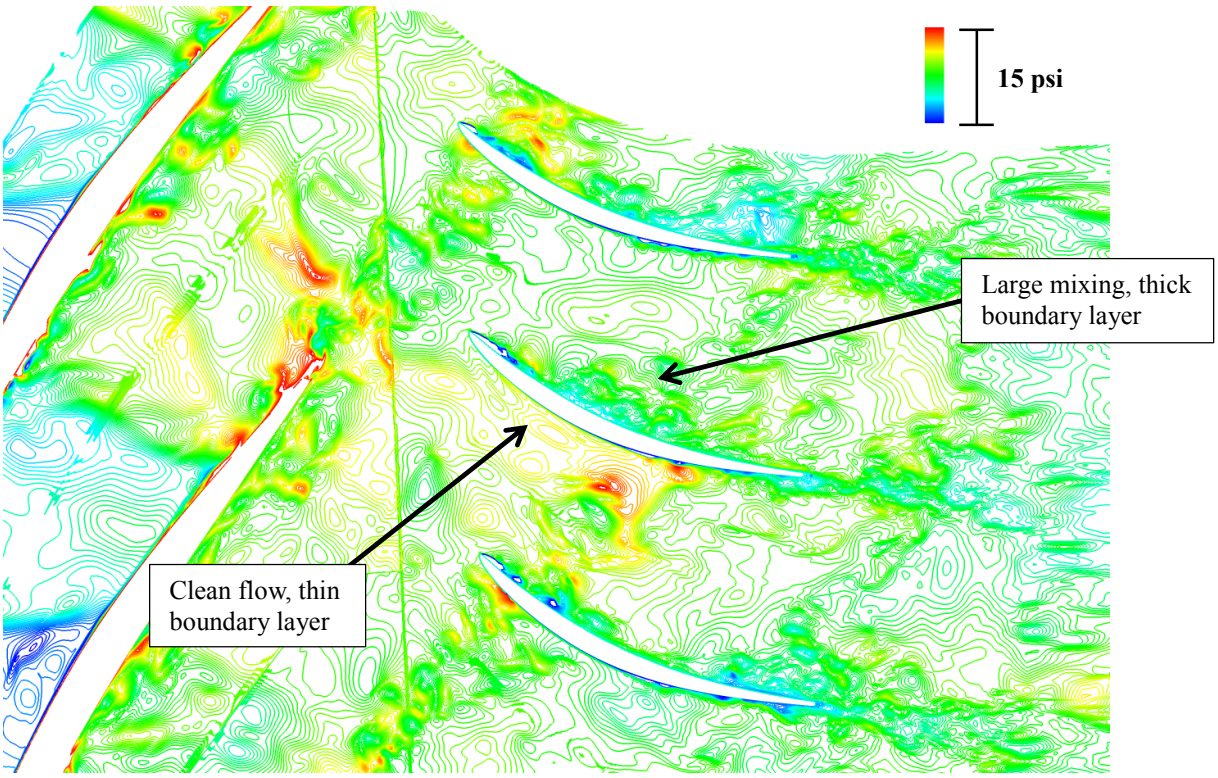

Figure 18: Instantaneous distribution of total pressure inside stator, mid-span

However, this negative tangential velocity component decays rapidly as the rotor wake enters the stator passage. Both the measurement and the LES show that the total temperature is significantly higher on the pressure side (Figure 15). As the blades are almost adiabatic, this asymmetric distribution of total temperature at the stator exit must be due to some inviscid redistribution as rotor wake sweeps through the stator. Kerrebrook and Mikolajcak [1970] attributed this phenomena to the jet velocity in the rotor wake. As shown in Figure 16, the jet velocity in the wake decays fast when it enters the stator passage. Instantaneous flow structures shown in Figures 7 and 16 implies that the jet velocity in the rotor wake does not push wake fluid directly toward pressure side of the stator. Instantaneous vorticity contours inside the stator passage are shown in Figure 17. Two yellow lines in Figure 17 show that rotor wake is much wider near the pressure side than near the suction side. Counterclockwise rotating vortices are generated near the suction surface when rotor wake hits the suction surface boundary layer due to the jet velocity in the rotor wake. The current LES results show that these vortices travel toward the pressure side as marked in Figure 17. Similar vorticities were also observed by Valkov and Tan [1995] in their two-dimensional incompressible rotor/stator interaction study. Counterclockwise rotating vortices pushes wake fluid into the free stream behind the rotor wake, which results in wider wake toward the pressure side. When total temperature is measured near the pressure side of the stator near the trailing edge, one can see more wake fluid pass through. On the other hand, one can observe more free stream fluid near the suction side. Widening of rotor wake near the pressure side by the counterclockwise rotating vortices seems to be the actual mechanism of the observed redistribution of total temperature during the rotor wake/stator interaction. Examination of the flow structure in the spanwise direction indicates the formation of vortices similar to Görtler vortices [1954] on the pressure side of the stator.

Instantaneous distribution of total pressure in the stator passage is shown in Figure 18. The instantaneous total pressure distribution in Figure 18 shows many important unsteady flow features as the rotor wake passes through the stator passages. As marked in Figure 18, the suction side of the stator blade shows much cleaner flow with the thin blade boundary layer between rotor wakes. On the other hand, flow near the pressure side of the blade shows a large accumulation of loss and a thick blade boundary layer between rotor wakes. As shown in Figure 18, the development of flow near the blade surface is drastically different between the suction side and the pressure side of the blade. The main difference between the suction side and the pressure side of the blade near the leading edge is that the pressure side of the blade has concave curvature while the suction side has convex curvature. Curvatures of the stator blade and jet velocity in the wake are illustrated in Figure 19. Effects of longitudinal curvature on the stability of a curved wall boundary layer have

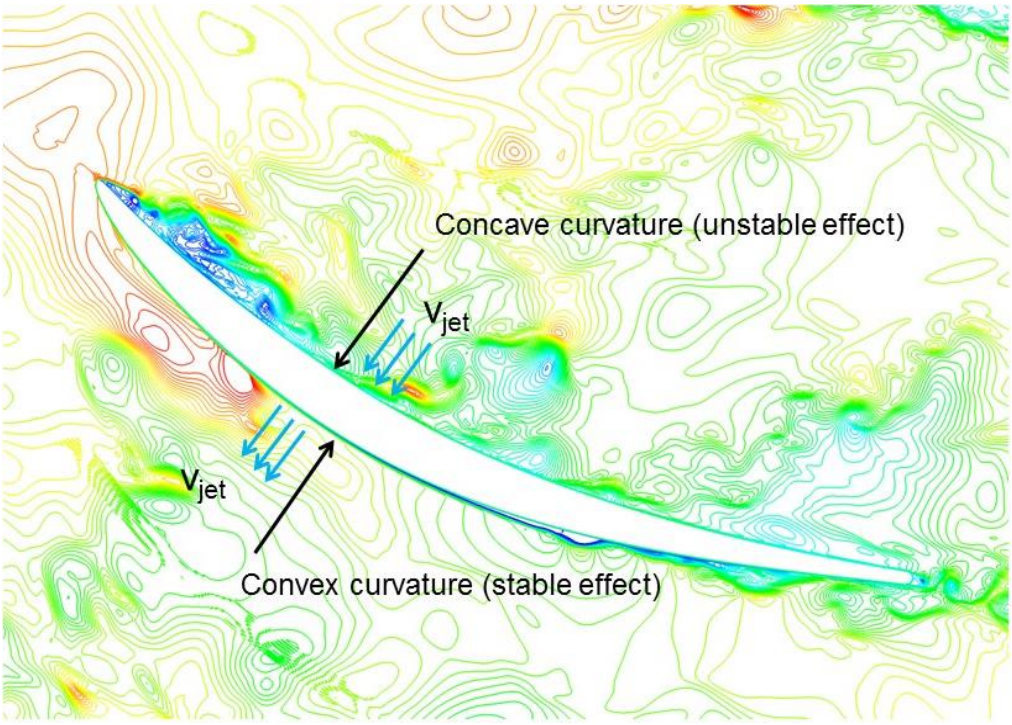

Figure 19: Curvature of the stator blade, jet velocity, and instantaneous total pressure contours

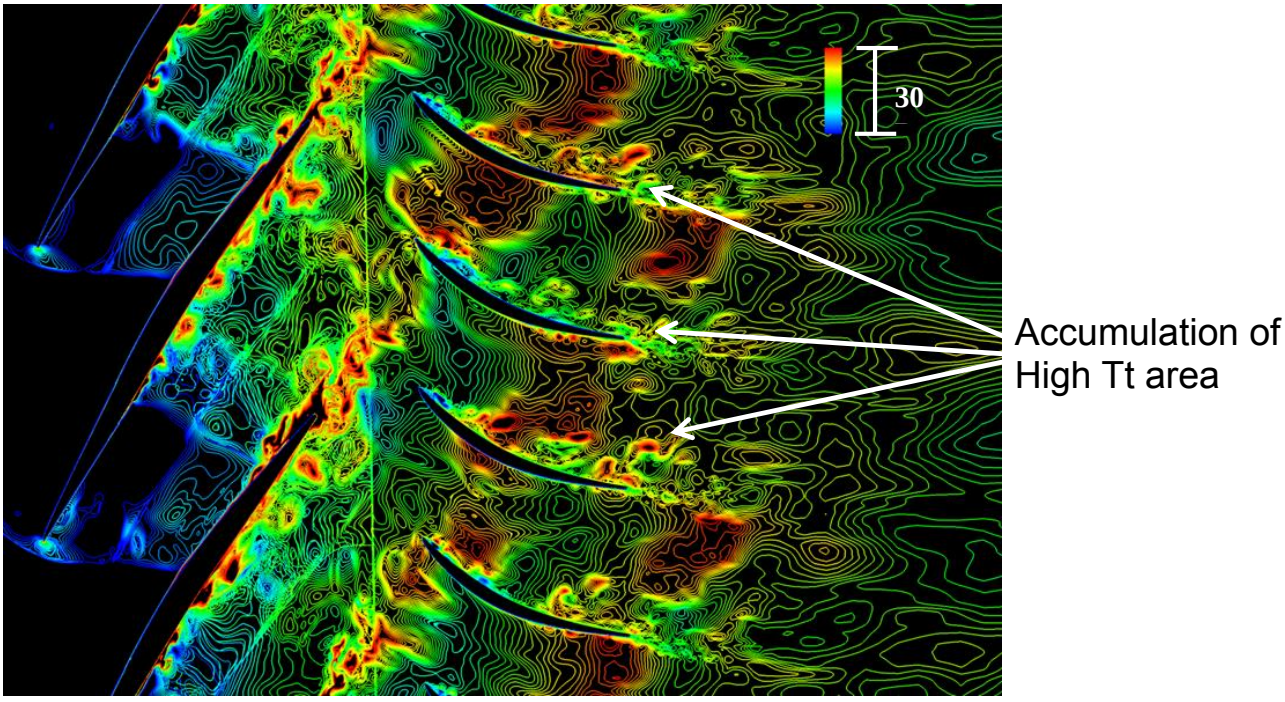

Figure 20: Instantaneous distribution of total temperature, mid span

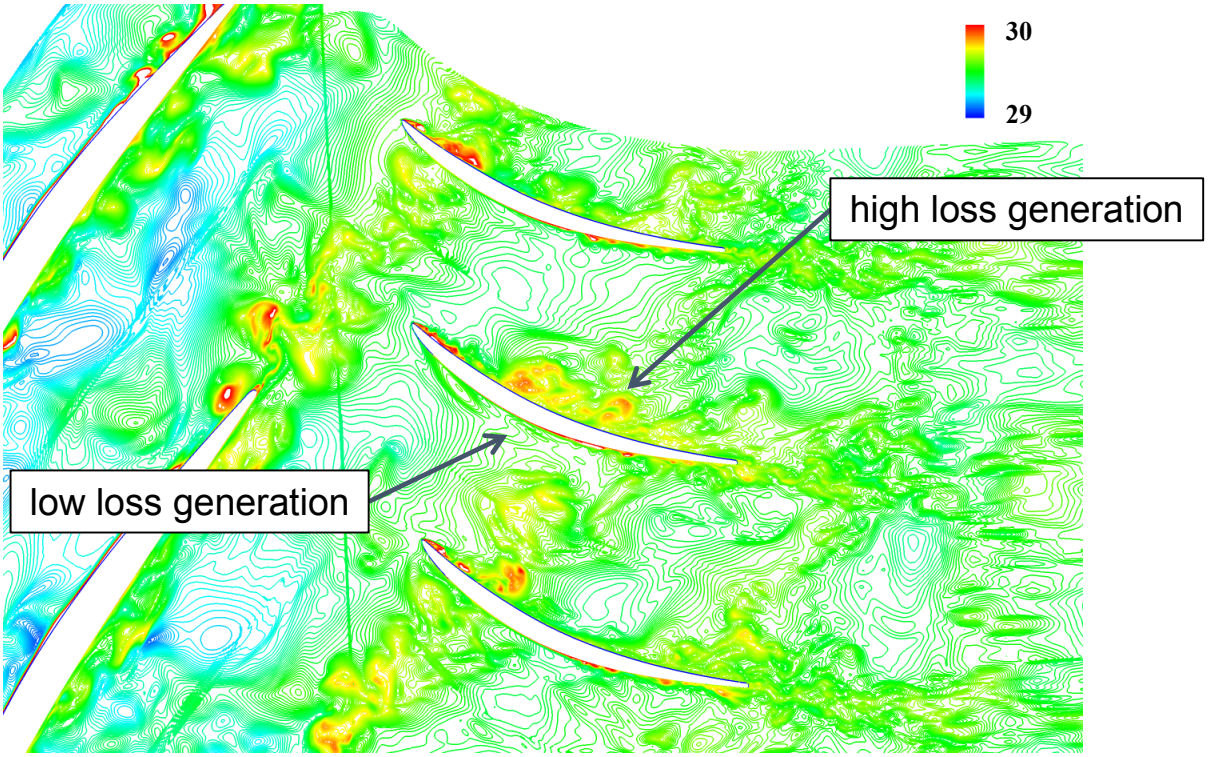

Figure 21: Instantaneous distribution of entropy generation, mid span

been studied since Prantl [1929] proposed following corrective multiplier on the mixing length.

$$\frac{l}{l_0} \equiv F = 1 - \frac{1}{4}\left(\frac{U/R}{\partial U/\partial y}\right) \qquad (1)$$

where R is the streamline radius of curvature.

Many experimental studies indicated that the actual curvature effects are much larger than initially estimated. Unsteady flow field in the stator from LES indicates that the jet velocity in the rotor wake, which is pointing to the pressure side in the approaching rotor wake, amplifies the effects of the longitudinal curvature on the flow development near the stator blade. The rotor wake passing near the suction surface is stabilized by both the convex curvature of the blade and the jet velocity in the wake. On the other hand, flow passing near the pressure side of the stator becomes unstable by the concave longitudinal curvature and the jet velocity, resulting in a thicker boundary layer and a larger loss due to the concave curvature and the jet velocity of the wake.

Instantaneous total temperature distribution inside the stator passage from LES is shown in Figure 20. The total temperature distribution in Figure 20 shows accumulation of areas with high total temperature near the pressure side at the trailing edge. This area with high total temperature on the pressure side near the Stator 1 exit shown in Figure 20 is caused by the inviscid redistribution of the rotor wake and high mixing near the pressure side.

Instantaneous contours of the entropy generation in the stator from LES are shown in Figure 21. With the higher total temperature along with the lower total pressure on the pressure side of the stator, a high loss region is created on the pressure side of the stator. The additional loss generation on the pressure side of the stator is a direct result of the rotor wake chopping by the stator.

Various analysis tools based on RANS and URANS do not calculate the high loss on the pressure side of the stator (Lurie and Breeze-String Fellow [2015]), resulting in the prediction of much higher compressor efficiency. URANS simulation of the current compressor stage with a fairly fine computational grid does not show the high loss region on the pressure side of the stator (To [2015]). It appears the rotor wake decays much faster with the URANS even with a finer grid. Also, vortex structures in the wake and curvature effects are not calculated with the URANS due to turbulence modeling. To be able to predict this complicated flow phenomenon, any analysis tool needs to calculate both the transport of the rotor wake and the curvature effect of the blade accurately.

CONCLUDING REMARKS

LES is applied to identify loss sources in an advanced GE highly loaded, high reaction, transonic one and a half stage compressor. Previous investigations have shown that various tools based on RANS and URANS predict significantly higher efficiency than the measurement. The applied LES calculates higher total temperature with lower total pressure on the pressure side of the stator. Consequently, high loss generation is calculated on the pressure side of the stator. This high loss generation on the pressure side of the stator has not been calculated by various tools based on RANS and URANS. Test data seem to confirm the LES results. Detailed examination of the calculated LES flow field along with the measurement indicates that this high loss is the result of the interaction of the rotor wake with the stator blade.

As explained by Kerrebrock and Mikolajczk [1970], rotor wakes have a velocity component (jet velocity) that pushes the rotor wake toward the pressure side of the stator blade. The rotor wake has higher total temperature and higher total pressure in the stator frame compared to those in free stream. Migration of the wake fluid with high temperature toward the pressure side of the stator blade occurs only because the rotor wake is chopped by the stator blades. The current LES analysis shows that the jet velocity in the wake decays fast when the wake enters the stator passage. The calculated unsteady flow field from LES shows that flow near the pressure side of the stator is less stable and has a thick boundary layer even after the rotor wake sweeps through the blade. On the other hand, flow near the suction side is much more stable and has a very thin boundary layer developing even after the rotor wake sweeps the stator blade.

We asked the simple question: Why does the rotor wake interact very differently between the pressure side and the suction side (higher total temperature and lower total pressure on the pressure side of the stator exit)?

The current LES analysis shows that:

1. Counterclockwise rotating vortices are generated when the rotor wake hits the suction side blade boundary layer due the jet velocity in the wake. The rotor wake becomes significantly wider near the pressure side than near the suction side as these vortices push wake fluid toward the free stream behind the wake. Consequently, unsteady flow near the pressure side is covered with more wake fluid, which has higher total temperature, than near the suction side. This is why higher total temperature is measured near the pressure side at the stator exit.

2. The destabilizing effect of the concave curvature on the pressure side makes the boundary layer thicker with high loss. On the other hand, the stabilizing effect of the convex curvature on the suction side of the stator blade makes flow near the suction side clean with a thinner boundary layer, even after the rotor wakes pass through. This explains why lower total pressure is observed on the pressure side near the stator exit. The jet velocity in the rotor wake in the stator frame seems to magnify the effects of the longitudinal curvature.

Further study is necessary to determine the exact amount of contributions from the inviscid redistribution of wake flow and the enhanced wake mixing near the stator pressure side in the total loss generation. As the basic mechanism of loss generation in such a highly loaded compressor stage is understood better, the optimum design strategy for better performance could be developed.

ACKNOWLEDGMENTS

The author gratefully acknowledges the support of this work by the NASA ERA program. Many helpful discussions about the test results with the NASA/GE experimental team (S. Prahst, S. Kulkarni, K. Sohn, and H. Shin) and very instructive discussions with D. Lurie and A. Breeze-Stringfellow about the GE data matching analysis are greatly appreciated.

REFERENCES

Germano, M., Piomelli, U., Moin, P., and Cabot, W. H., 1991, "A Dynamic Subgrid-Scale Eddy-Viscosity Model," Journal of Fluid Mechanics, Vol. A3, pp. 170-176.

Görtler H., 1954, "On the three-dimensiaonal instability of laminar boundary layers on concave walls," NACA TM 1375.

Gourdain, N., 2013, "Validation of Large Eddy Simulation for the Prediction of Compressible Flow in an Axial Compressor Stage, ASME paper GT 2013-94550.

Hah, C. and Shin, H., 2012, "Study of Near –Stall Flow Behavior in a Modern Transonic Fan with Compound Sweep," ASME Journal of Fluids Engineering, Vol.134, pp.071101-071107.

Hah C. and Katz J., 2014 "Investigation of Tip Leakage Flow in an Axial Water Jet Pump with Large Eddy Simulation," proceedings of 30th Naval Hydrodynamics Symposium, Hobart, Australia.

Kerrebrock J.L. and Mikolajczk A. A., 1970, "Intra-Stator Transport of Rotor Wakes and Its Effect on Compressor Performance," ASME Journal of Engineering for Power, Vol.92, pp 359-368.

Knobbe, H., and Nicke, E., 1012 "Shock Induced Vortices in Transonic Compressors: Aerodynamic Effects and Design Correlations," ASME Paper, GT2012-69004.

Lurie, D.P. and Breeze-Stringfellow, A, 2015, "Evaluation of Experimental Data from a Highly Loaded Transonic Compressor Stage to Determine Loss Sources," ASME Paper GT2015-42526.

Nolan, S.P.R., Botros, B.B., Tan C.S., Adamczyk, J.J., Greitzer, E.M., and Gorrel, S.E., 2009, "Effects of Upstream Wake Phasing on Transonic Axial Compressor Performance," ASME Paper, GT2009-59556.

Padogiannis, D., Duchane, F., Gicquel, L., Wang, G., and Moreau, S, "Large Eddy Simulation of High Pressure Turbine Stage: Effects of Sub-Grid Scale Modeling and Mesh Resolution," ASME paper GT2014-25876.

Prahst, P.S., Kulkarni, S., and Sohn, K.H., 2015, "Experimental Results of the First Two Stages of an

Advanced Transonic Core Compressors Under Isolated and Multi-Stage Conditions," ASME Paper, GT2015-42727.
Prandtl, L., 1929, "Effects of stabilizing forces of turbulence," NACA TM 625.
Smith L. H. Jr., 1966, "Wake Dispersion in Turbomachines," ASME Journal of Basic Engineering, Vol. 88.
Smith L. H. Jr., 2010, Private communication.
To, W., 2015, Private communication.
Van Zante, D.E., Adamczyk, J.J., Strazisar, A.J., Okiishi, T.H., 2002, "Wake Recovery Performance Benefit in a High Speed Axial Compressor," ASME Journal of Turrbomachinery, Vol.124, pp275-284.
Valkoy, T. and Tan C.S., 1995, "Control of the Unsteady Flow in a Stator Blade Row Interacting with Upstream Moving Wakes." ASME Journal of Turbomachinery, Vol.117, pp 97-117.
Zaki, T, Wissink, J., Durbin, P.A., and Rodi, W., 2010, "Direct Numerical Simulations of Transition in a Compressor Cascade: the Influence of Free-Stream Turbulence," J. of Fluid Mechanics, Vol. 665, pp 57- 98.